Geofísica Internacional (1998), Vol. 37, Num. 2, pp. 113-126

Mean flow stability in a model of the eastern North Pacific ocean

Guillermo Auad[1] and Alejandro Parés-Sierra[2]

[1] *Climate Research Division, Scripps Institution of Oceanography, La Jolla, CA, USA.*

[2] *Centro de Investigación Científica y Educación Superior de Ensenada, Ensenada, B. C., México.*

Received: August 1, 1996; accepted: August 6, 1997.

RESUMEN

Datos de estratificación y corriente media de un modelo cuasigeostrófico de ocho capas de la Corriente de California son usados para resolver el problema de estabilidad lineal asociado. Se obtiene, al resolver un problema de autovalores complejos la frecuencia, rapidez de fase, velocidad de grupo, razón de crecimiento y estructura vertical. Se corren siete experimentos para estudiar la influencia de las diferentes condiciones de frontera (fondo plano o inclinado), dirección media de la corriente, amplitud, latitud y mecanismos de fricción en las características de las ondas de Rossby. Usando valores de la frecuencia de flotabilidad características del Pacífico Nororiental encontramos que la resolución vertical es crucial para determinar los efectos de la topografía y fricción de fondo en la estabilidad del flujo básico. La estructura vertical del flujo medio tiene un efecto importante en la escala de decaimiento exponencial. Esta escala de decaimiento de las diferentes áreas de la región de la Corriente de California varía entre 144 y 374 días para las ondas más inestables. La estructura vertical de nuestra solución de onda (amplitud y fase) es afectada perceptiblemente por la disipación usada en el modelo. Las características del primer modo baroclínico de la onda estable son cualitativamente y cuantitativamente similares a las obtenidas por Kang *et al.* (1982) usando datos hidrográficos de la Corriente de California. La inclusión de topografía de fondo lleva a una moderada redistribución de frecuencias en el espacio de número de onda y a más altas velocidades de grupo.

PALABRAS CLAVE: Ondas de Rossby, estabilidad, modelación numérica, Corriente de California.

ABSTRACT

Mean flow and stratification data obtained from an eight-layer quasigeostrophic model of the California Current System are used to feed a linearized model, from which a stability problem is solved. Frequencies, phase speeds, group velocities, growth rates and vertical structures are obtained after solving a complex eigenvalue problem. Seven runs are implemented to study the role played by different vertical boundary conditions (flat and sloping bottom), mean flow direction and amplitude, latitude and frictional mechanisms on the Rossby wave characteristics. For values used of buoyancy frequency as found in the Northeastern Pacific, the vertical resolution is crucial in determining the effects of bottom topography and bottom friction on stability of the basic flow. The vertical structure of the mean flow has an important effect on the determination of the e-folding-time. The e-folding times of different areas in the California Current System region range from 144 to 374 days for the most unstable waves, as found by other authors using different data and models. The vertical structure of our wave solutions (amplitudes and phases) are noticeably affected by dissipation. The first baroclinic mode stable waves show a good qualitative and quantitative agreement with those obtained from hydrographic data for the California Current by Kang *et al.* (1982). The inclusion of bottom topography leads to a moderate redistribution of frequencies in the wavenumber space and to higher group velocities.

KEY WORDS: Rossby waves, stability, numerical model, California Current.

I.-INTRODUCTION

Rossby waves can be generated by seasonal fluctuations in longshore wind stress, by time-dependent Ekman pumping forced by the annual oscillations of the wind stress curl, by Kelvin wave activity and by barotropic and baroclinic instabilities. Baroclinic instability may have linear and nonlinear contributions (see Auad *et al*. 1991, hereafter A91, Pedlosky 1979). Linear contribution dominate the generation of waves over most of the California Current System (CCS)(A91).

We approach the Rossby wave problem, both stable or unstable, by solving the eigenproblem associated with the quasi-geostrophic equations and its vertical boundary conditions. Rossby waves are assumed to propagate on an infinite horizontal ocean with depth-dependent mean flow and stratification. The three-dimensional mean flow structure is obtained from a non-linear model (A91). This structure shows a good agreement with historical descriptions of the CCS. For example, the California Current, the Davidson Current, the California Undercurrent and the Southern California Eddy were all present in the model solutions. In addition, the CCS dynamics and their seasonal fluctuations as described in Lynn and Simpson (1988) were also reproduced by the model.

First we determine the period, wavelength, growth rate and vertical structure of Rossby waves from a two-year run of a non-linear model presented by Holland and Vallis (1995) and discussed in A91. The depth-dependent stratification is

the same which was used to obtain the mean flow from the non-linear model. Further, we study the spatial variability of the wave properties in the CCS by feeding the linearized model with the same parameters and physical processes used in the non-linear model. Finally, we compare the wave scales of the linearized model in this paper to those obtained in the non-linear model (A91), and we compare the wave properties obtained here with those reported by other authors. The response of stratification and mean flow to changes in dissipation and bottom conditions will be discussed. An eight-layer linearized quasi-geostrophic model, that includes lateral and bottom friction is used. We assume that baroclinic instability is the dominant source of eddy kinetic energy, since eastern boundary currents have a weak horizontal shear. As shown by Auad (1989, hereafter A89), the amount of eddy kinetic energy produced by baroclinic instability (linear plus non- linear) is at least one order of magnitude larger than that due to barotropic instability in the areas we are studying. Assuming an absence of horizontal shear, is consistent with our selection of a constant bottom slope. The vertical resolution of the model is fine enough to represent continuous model energetics. Lee and Niiler (1987), suggest a minimum of six layers for the North East Pacific.

An early study of the kind proposed here was due to Kang *et al*. (1982), who used 2-layer continuous models and the mean flow was allowed to change direction with depth. They computed a dispersion relation for first-baroclinic-stable-mode Rossby waves at 35°N - 132.5°W. For a southeastward flow with a vertical shear of 7 cm s^{-1}, a two-layer inviscid model, they found that the most unstable wave propagates southward with a wavelength of 470 km, a period of 243 days and an e-folding time of 52 days. Lee and Niiler (1987) evaluated the complex dispersion relation for quasi-geostrophic waves in the Eastern North Pacific, west of 130° W. In their area V, west of our areas I and II, (see Figure 1), they found that the most unstable wave propagates southward with a wavelength of 180 km, a period of 528 days, and an e-folding time of 162 days when the surface mean flow is about 2 cm s^{-1} southeastward. For a three-layer quasi-geostrophic box model Lee (1988) showed that in a westward mean flow of 2 cm s^{-1}, the most unstable wave propagates westward with a wavelength of 175 km, a period of 226 days, an e-folding time of 160 days. For a southward mean flow the most unstable wave propagates also southward but has an e-folding time of about 210 days. All these results show good agreement with the observed variability.

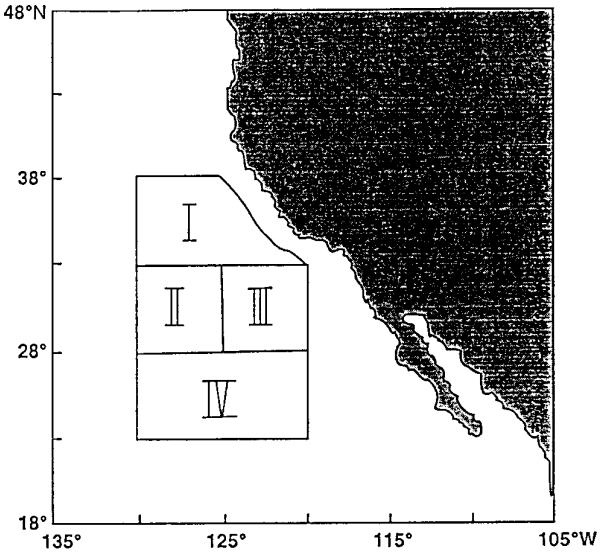

Fig. 1. Areas where all seven runs were performed. The mean flow used in each is averaged for each area.

Table 1

Model Parameters common to all seven runs

Summary of Model Parameters

Layer thickness	100.,150.,250.,450.,650.900,1150.,1350.*m*
Reduced gravities	0.07061, 0.008196, 0.008389, .0.005521
	0.002170, 0.0005094, 0.00006908 *m* s^{-2}
f_o	7.943 x $10^{-5}s^{-1}$
β	1.92 x $10^{-11}m^{-1}s^{-1}$
Earth's radius	6.37 x $10^{6}m$

II. THE MODEL

a. Data

The data that provides the mean values defining the eigenproblem described below correspond to the years 1979-1980. They were generated by the eight-layer limited area quasi-geostrophic numerical model by Holland and Vallis (1995). Results from this model for the same two-year period were analyzed in A91. The model is wind driven by the Fleet Numerical Oceanographic Center (FNOC) wind stress curl. It includes lateral Laplacian friction and bottom linear friction. It also includes realistic topography and it is embedded in another numerical model that occupies almost the whole North Pacific Ocean but has coarser horizontal resolution (one-sixth of a degree vs. one degree).

The region discussed in this paper is shown in Figure 1. In Table 1 we present the reduced gravities and layer thicknesses, while in Figure 2 we show the four different vertical structures of the mean flow studied in this paper.

b. Governing Equations

The perturbed and linearized quasi-geostrophic equations for a two-layer ocean are given in Pedlosky (1979) and Kang *et al.* (1982) for a spiraled inviscid flow. Lee and Niiler (1987) introduced lateral Laplacian friction and presented the derivation of an N-level model. All these authors impose a rigid lid at the sea surface (z=0) and a flat bottom at the lower

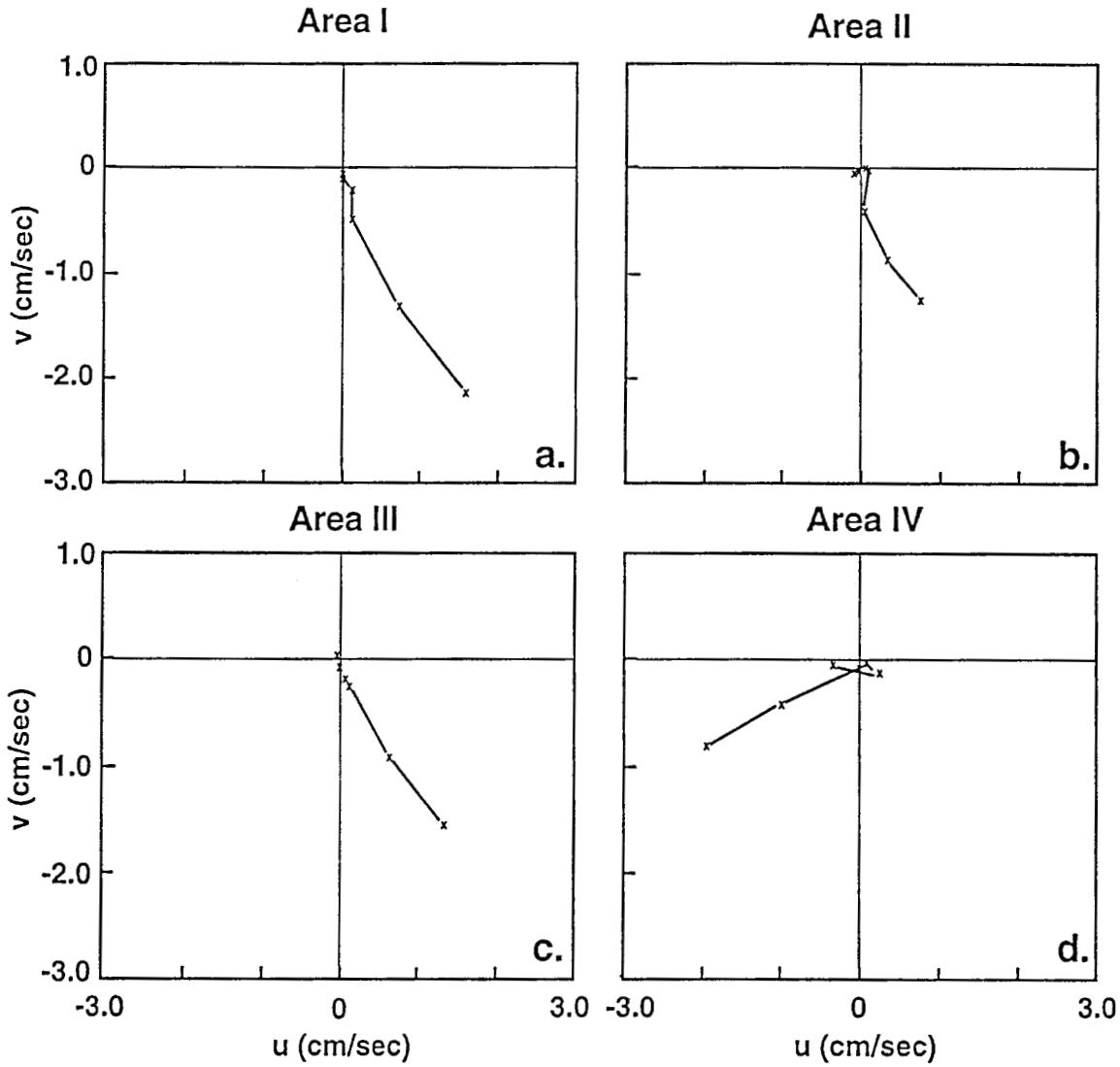

Fig. 2. Vertical structure of the mean flow for all four areas shown in Fig. 1. a) Area I b) Area II c) Area III d) Area IV. Each star corresponds to a different layer. Larger velocities are higher up in the water column.

level (z=-H). Following Lee and Niiler (1987) we derive the case in which a large-scale topography gradient (bottom boundary condition) and linear bottom friction are included. The linearized evolution for the quasi-geostrophic streamfunction (φ), and its vertical boundary conditions, are given by

$$\left(\frac{\partial}{\partial t}+\bar{u}\frac{\partial}{\partial x}+\bar{v}\frac{\partial}{\partial t}\right)\left[\nabla^2\varphi+\frac{\partial}{\partial z}\left(\frac{f_0^2}{N^2}\frac{\partial\varphi}{\partial z}\right)\right]+\beta\frac{\partial\varphi}{\partial x}$$

$$-\frac{\partial}{\partial z}\left(\frac{f_0^2}{N^2}\frac{\partial\bar{u}}{\partial z}\right)\frac{\partial\varphi}{\partial x}-\frac{\partial}{\partial z}\left(\frac{f_0^2}{N^2}\frac{\partial\bar{v}}{\partial z}\right)\frac{\partial\varphi}{\partial y}=-A_m\nabla^4\varphi+\varepsilon\nabla^2\varphi\delta_{-H,z} \qquad (1)$$

$$w'=J(\varphi,b)\delta_{-H,z} \quad \text{at} \quad z=0,-H, \qquad (2)$$

where $\bar{u}$ and $\bar{v}$ are the zonal and meridional components of the mean flow, f_0 is the Coriolis parameter, β is the meridional gradient of the Coriolis parameter, A_m is the lateral Laplacian friction coefficient, ε is the bottom friction coefficient, δ is Kronecker's delta, *b* is the bottom topography, *w* is the vertical velocity, *J* is the Jacobian operator and *N* is the buoyancy frequency. Condition (2) implies that,

$$\left(\frac{\partial}{\partial t}+\bar{u}\frac{\partial}{\partial x}+\bar{v}\frac{\partial}{\partial t}\right)\frac{\partial\varphi}{\partial z}-\left(\frac{\partial\bar{u}}{\partial z}\frac{\partial\varphi}{\partial x}+\frac{\partial\bar{v}}{\partial z}\frac{\partial\varphi}{\partial y}\right)+$$

$$\frac{N^2}{f_0}J(\varphi,b)\delta_{-H,z}=0$$

Table 2

Model Parameters for the different runs: b_x is the zonal topographic gradient, b_y is the meridional topographic gradient, ε is the the bottom friction coefficient, A_m is the Laplacian lateral friction coefficient and A_4 is the biharmonic lateral friction coefficient.

Experiments	Area	b_x	b_y	ε(s^{-1})	Am(m^2S^{-1}) [A_4(m^4S^{-1})]
1	I	$1x10^{-3}$	$5x10^{-4}$	$1x10^{-7}$	200
2	I	0	0	$1x10^{-7}$	200
3	I	$1x10^{-3}$	$5x10^{-4}$	$1x10^{-7}$	[$8x10^9$]
4	I	$1x10^{-3}$	$5x10^{-4}$	0	200
5	II	$1x10^{-3}$	$1x10^{-4}$	$1x10^{-7}$	200
6	III	$8x10^{-4}$	$1x10^{-4}$	$1x10^{-7}$	200
7	IV	$1x10^{-3}$	$1x10^{-4}$	$1x10^{-7}$	200

$$\text{at} \qquad z = 0, -H. \tag{3}$$

We seek normal mode solutions of the form

$$\varphi(x,y,z,t) = \mathrm{Re}\left\{\phi(z)\exp\left[i(kx+ly-\omega t)\right]\right\} \tag{4}$$

where ϕ(z) is the complex amplitude, k and l are zonal and meridional wavenumbers respectively, and ω is the wave frequency.

From (1) and (4) we obtain,

$$(U^*-c)\left\{\frac{d}{dz}\left(\frac{f^2}{N^2}\frac{d\phi}{dz}\right)-K^2\phi\right\}+\left\{\beta^*-\frac{d}{dz}\left(\frac{f^2}{N^2}\frac{dU^*}{dz}\right)\right\}\phi =$$

$$-(A_mK^2+\varepsilon\delta_{-H,z})iK\phi \tag{5}$$

and from the vertical boundary conditions

$$(U^*-c)\frac{d\phi}{dz}-\left(\frac{dU^*}{dz}-\frac{N^2}{f_0}B^*\delta_{-H,z}\right)\phi = 0 \quad \text{at} \quad z = 0, -H \tag{6}$$

where

$$U^* = \frac{\bar{u}k+\bar{v}l}{K}, \quad \beta^* = \frac{\beta k}{K}, \quad c = \frac{\omega}{K}, \quad B^* = \frac{\vec{K}x\nabla bl_z}{K}, \quad K = \left|\vec{K}\right|$$

and $\vec{K}$ =(k,l).

The discretization scheme used to solve the complex eigenvalue problem (5) and (6) is described by Lee and Niiler (1987). Our equations differ from theirs in the bottom boundary condition and in the bottom friction term. The present linearized model is a discretization in eight levels of a continuous quasi-geostrophic model which is exactly equivalent to an eight layer quasi-geostrophic model (Pedlosky 1979). If biharmonic friction is used instead of Laplacian friction, the lateral friction term takes the form

$$(A_4K^4-\varepsilon\delta_{-H,z})iK\phi, \tag{7}$$

where A_4 is the biharmonic lateral friction coefficient defined in Table 2. Other authors have dealt in detail with the issue of Laplacian versus biharmonic friction (e.g. Harrison 1980). Here we only show the main features of the most unstable wave for a biharmonic frictional ocean (Table 3).

The external forcing term is not included in our calculations. At quasi-geostrophic scales it only enters the stability problem by defining the structure of the mean flow (Pedlosky 1979). Thus a mean meridional flow, $\bar{v}$, would not exist without a mean wind stress curl.

Table 3

Characteristics of the Most Unstable Waves for all seven runs. T is the period, λ is the wavelength, C_r is the phase speed, T_e is the e-folding time, θ is the propagation direction and *Rd* is the deformation radius.

Experiments	T(days)	λ(km)	C_r(km day^{-1})	T_e (days)	θ(°)	R_d(km)
1	469	296	0.63	177	262	36
2	438	273	0.62	179	268	36
3	241	166	0.69	94	288	36
4	469	296	0.63	177	262	36
5	852	439	0.51	374	258	41
6	724	347	0.50	255	264	41
7	165	213	1.29	144	209	48

c. Experiments

We perform seven calculations to study the spatial inhomogeneities of the CCS wave field and its sensitivity to different boundary conditions, mean flows and frictional mechanisms. The parameters for each case are shown in Table 2. Zonal and meridional values of the large scale topography gradient, b_x and b_y, are typical for the selected areas, though we are mainly concerned with qualitative effects in comparison with the flat-bottom case.

Cases 1 and 5 to 7 show that different mean fields can affect stable or unstable Rossby waves. In Case 2 we discuss the topographic effect, while in case 3 we analyze the influ-

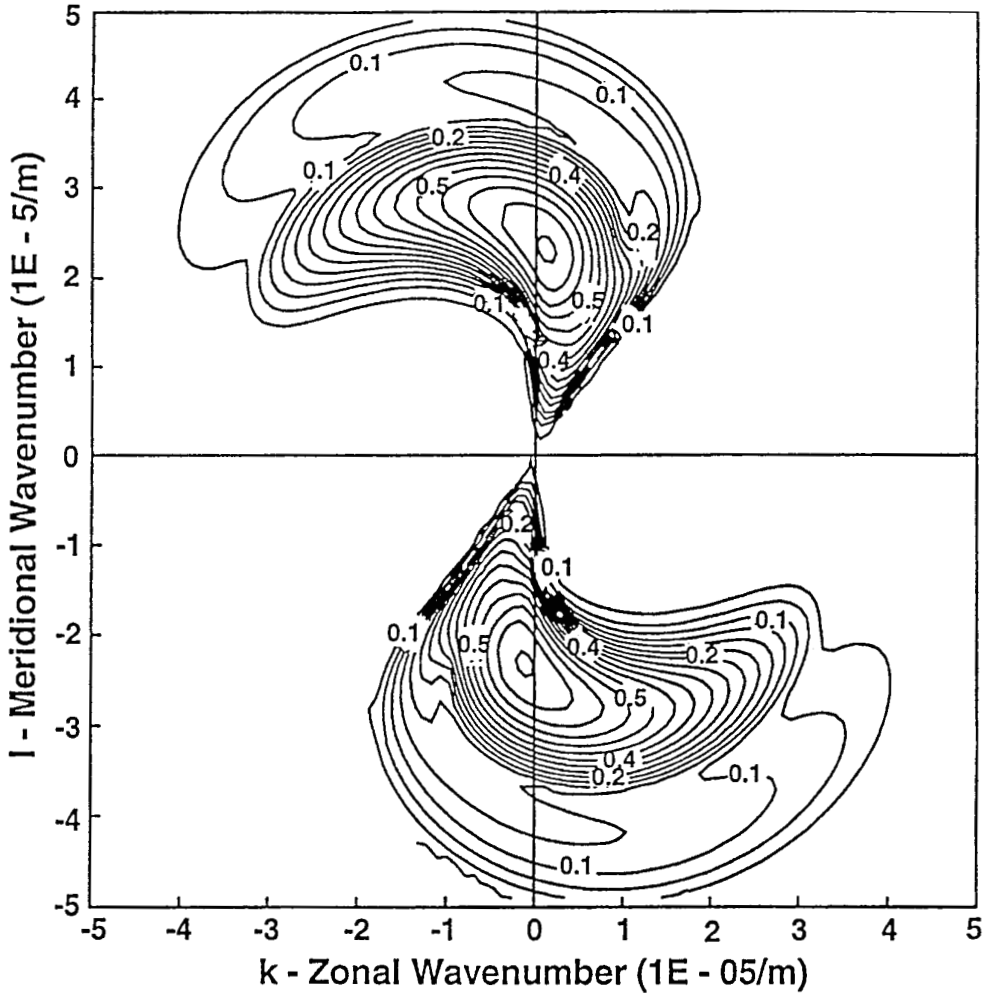

Fig. 3. Growth rates of unstable waves for Case 1 (sloping bottom, Area I). Contour Interval = 4 x 10^{-9} s^{-1}. The growth rate or imaginary part of the complex frequency is a measure of the wave instability. Its inverse, the e-folding time, is the time required for the wave to grow or decay *e* (=2.718...) times. Since we are interested in highly energetic waves, we only show here positive e-folding times, i.e. growing waves (see text for details on how to obtain growth rates).

ence of bottom friction on the perturbed field. We use the mean flow latitude data of area I to explore the physics of Cases 2 and 4. Runs 1 and 5 to 7 feature the same conditions which were used to obtain the mean field data, including the same stratification, frictional processes and coefficients and average bottom slope as in the non-linear numerical model of eq (5) and (6). We take Case 1 as the control case. In order to calculate ω and $\phi(z)$ in (4), we compute the complex eigenvalues c, (i.e. the complex phase velocities), and the eigenvectors $\phi(z)$ from the discretized version of equation (5) and (6) for an eight-layer system. The complex frequency is $\omega = \omega_r + i\omega_i$, where ω_r is the wave frequency and ω_i is the wave growth rate. The inverse of ω_i is often referred to as the e-folding-time, it is a measure of the wave ability to convert available potential energy from the mean field into eddy kinetic energy.

Unstable or stable waves are obtained depending on the sign of ω_i. For stable waves we set the viscosity coefficient to zero. For stable waves the distribution of frequencies in wavenumber space (dispersion relation) was very slightly affected by the inclusion of friction.

III. RESULTS

a. Case 1

This case refers to stable or unstable Rossby waves in Area 1 (see Figure 1). This is our control experiment. The parameters and physical mechanisms used for this experiment are the same ones as in the non-linear model.

Growth rates of unstable waves ($\omega_i > 0$) in Area I are

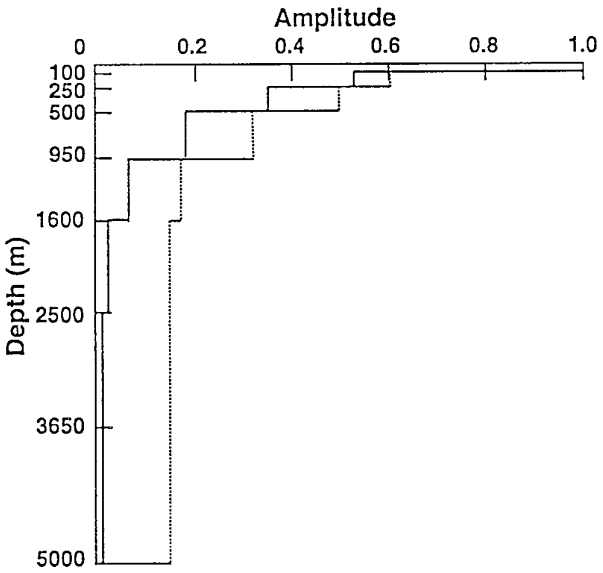

Fig. 4. Amplitude of the most unstable wave (MUW) for Case 1 (solid line) vs. the square root of the eddy kinetic energy (dotted line) obtained from the non-linear numerical model (both for Area I.) Both curves are normalized against their maximum values. The amplitude and phase of the MUW are obtained from the complex eigenvectors.

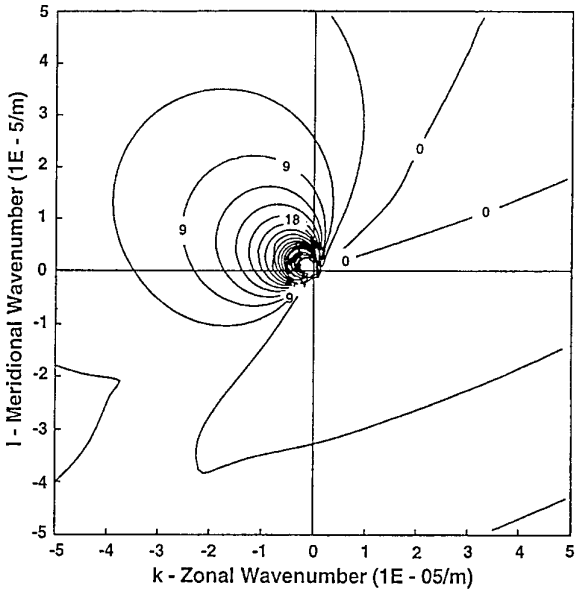

Fig. 5a. Dispersion relation for barotropic mode of stable waves (Case 1) (sloped bottom). Contour interval = 3×10^{-7} s^{-1}. This figure shows the wave frequency in the wavenumber space, i.e. a dispersion relation. Waves on the left hand side propagate westward (see text for details).

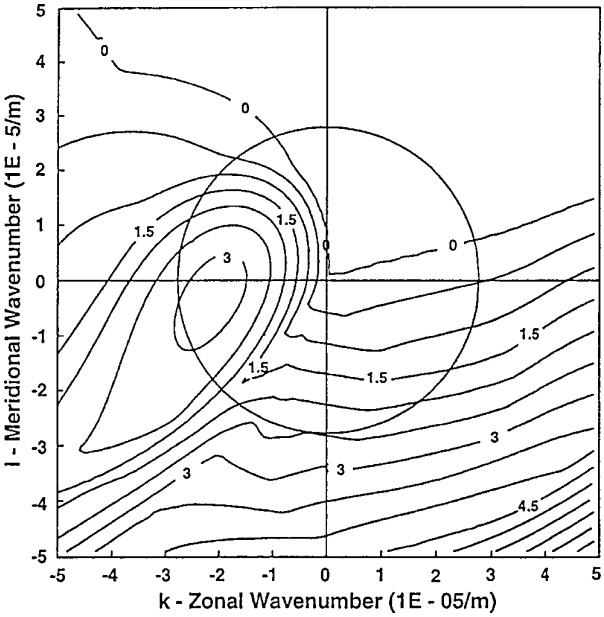

Fig. 5b. Dispersion relation for first baroclinic mode of stable waves (Case 1). The circle corresponds to the wavenumber associated with the deformation radius. Contour interval = 5×10^{-8} s^{-1}.

shown in Figure 3. These perturbations are generated by linear baroclinic instability (i.e., downgradient eddy fluxes of temperature), through the conversion of potential to kinetic energy. We consider the most unstable wave in more detail. This wave minimizes the stabilizing effect of beta and maximizes the projection of the eddy flux of temperature onto the mean temperature gradient (Pedlosky 1979, chapter 7). Thus the conversion of available mean potential energy into eddy kinetic energy is maximized.

Comparing Figure 3 and 2a we find that the most unstable wave (maximum growth rate) is not exactly aligned with the direction of the mean flow of the three upper layers, because it is not strong enough to overcome the beta effect. Kang *et al*. (1982) show that for mean flows nine times stronger than that of Area I, the most unstable wave is aligned with the mean flow direction. The destabilizing effect of the mean flow overwhelms the stabilizing effect due to beta, no matter what the direction of the mean flow is. The direction of propagation of unstable waves is closely determined by the mean flow rather than by the beta effect even for mean flows as weak as 2-3 cm/s. In fact, the observed propagation directions in the non-linear model was always in the third quadrant (i.e., l<0, k<0, A89). This might partly explain the spatial inhomogeneity of the eddy velocity field observed by A89. The inhomogeneity is increases by the sensitivity of Rossby waves to horizontally non-uniform mean flows as will be shown in Cases 5, 6 and 7.

In Figure 4 we show the amplitude of the most unstable wave compared to the amplitude obtained from the average eddy-kinetic energy calculated from the numerical non-linear model (A89). The overall shape of both curves is very

similar to each other. The similarity between the non-linear results of A91 and the present linear results is due to the dominance of linear baroclinic instability over non-linear baroclinic instability over most of the areas studied in both articles. Note that the most unstable wave in all calculations corresponds to the first baroclinic mode. The horizontal scale of these waves fits 10 to 30 times into the areas of study. Comparing different areas (i.e. different mean flows) will partly help to explain the horizontal spatial inhomogeneity observed in the model waves of A91.

The dispersion relations $\omega_r(k,l)$ for the barotropic and first baroclinic modes of stable Rossby waves are curves of constant ω in *K* space (Figure 5a, b). Group velocities are larger in the larger scales than in the smaller ones. Maximum group velocities for westward propagating waves are about 2.6 cm s^{-1} for the first internal mode. Large scales are more suitable for comparison with the real nonlinear case, since linear waves dominate the wavenumber spectrum for scales $K^{-1} >> K_E^{-1} >> R_d$ in the quasi- geostrophic formalism (Cushman-Roisin and Tang 1990). Here R_d is the radius of deformation. For $K^{-1} < K_E^{-1}$ the propagation is dominated by geostrophic turbulence and linear processes become of lesser importance. In this case the linear and non linear terms of the governing equations have the same amplitude when,

$$K_E^{-1} = L_\beta R_0 \tag{8}$$

where $L_\beta = f_0 / \beta$ and R_0 is the Rossby number. For scales larger than K_E^{-1} we should expect a better agreement with observations. For the present deformation radius (see Table 3) the transition wavenumber is 2.78 x 10^{-5} m^{-1} (wavelength of 226 km). The circle in Figure 5b corresponds to $K^{-1} = R_d$.

Comparing the first internal mode (Figure 5b) to the synthetic data and two-layer model (Figure 9) and to the hydrographic data and the continuous model (Figure 11), there is good qualitative and quantitative agreement. The two-layer model of Kang *et al.* (1982) uses a southeastward mean flow of 1.8 cm s^{-1} and their continuous model computations were made at 35° N - 132.5° W. The cut-off frequency for the first internal mode corresponds to a period of 226 days at wavenumber *K(-2.0,-0.1)* x 10^{-5} m^{-1}. Thus, observed variability with periods shorter than the cut-off period (226 days in this particular case), is unlikely to be interpreted in terms of Rossby wave variability. In the following we analyze topographic, frictional and mean flow effects.

b. Case 2

The effect of including a different bottom boundary condition is explored here. We consider a flat bottom ocean; all other conditions are unchanged with respect to Case 1. We compare our results from an 8-layer model with results from 2-layer models by other authors, in order to infer the role of vertical resolution on stable and unstable waves.

The distribution of the growth rates in wavenumber space does not change noticeably. The e-folding time of the most unstable wave (see Table 3) reflects an increase of 1.3% (about 2 days) with respect to Case 1. Thus, the stability of the flat bottom case is not significantly different from that of of a bottom sloped ocean (Case 1). A similar result was obtained for area IV with a flat bottom (not shown). However, numerical experiments using two-layer models (e.g., Robinson and McWilliams, 1974; Holland and Schmitz, 1985; Walls, personal communication) suggest that bottom topography may play a more important role in the determination of the stability properties.

The amplitude and phase of the most unstable wave are shown in Figure 6a, b. The inclusion of topography in Case 1 shows a tendency to trap energy above the main thermocline (500 m). The most unstable wave in the sloping bottom case presents more a less depth-dependent phase below the main thermocline than does the most unstable wave in the flat-bottom case. A positive east-west bottom slope (e.g. off California), increases the β effect which leads to shorter and more barotropic waves. If the sign of the topography gradient is reversed and a more baroclinic wave with respect to the flat bottom case resulted.

The dispersion relations for the external and first internal stable modes are shown in Figure 7. The effect of topography is obviously stronger in the external mode. The inclusion of topography in Case 1 shows a general increase of about 20% in the group velocities for both modes and of the phase velocity in the external mode. Phase velocities in the first internal mode show small changes. Comparing the first internal mode (Figure 7b) with Figures 9a and 11 from Kang *et al.* (1982), the agreement is now better than in Case 1 (Figure 5b). The first internal mode cut-off period was 238 days at the wavenumber *K=(-2.2, -0.6)*x10^{-5}. m^{-1}.

c. Cases 3, 4, 5 and 6.

Case 3, a biharmonic frictional ocean for Area I, has been extensively studied by several authors (e.g., Harrison, 1980). Here we only show, for reference, the characteristics of the most unstable wave.

In Case 4 the bottom friction coefficient is set to zero. This experiment shows that bottom friction may be neglected when the vertical structure of the density field is properly resolved. The exception is for weakly stratified seas where the bottom friction effects is not confined to a small portion of the vertical column. In Cases 5 and 6 we study the effects of different mean flows and latitudes on the stability and dispersion properties of the associated quasi-geostrophic variability.

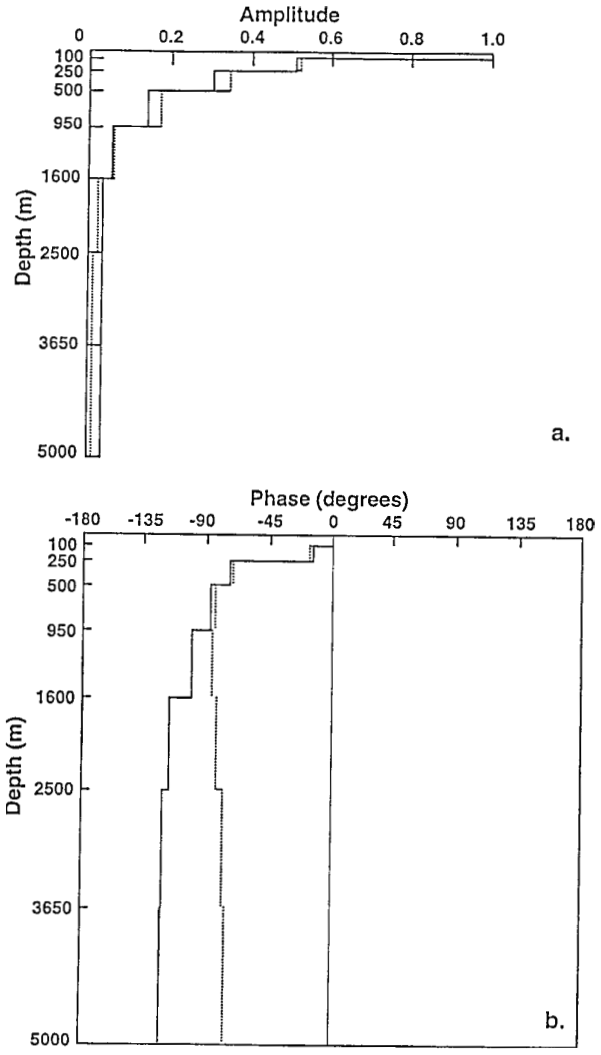

Fig. 6. a) Amplitude vs. depth of the MUW for the flat bottom (Case 2, solid line) vs. the MUW of the sloping bottom (Case 1, dotted line), b) As in a) but for phase vs depth.

The inclusion of an Ekman bottom layer does not significantly affect the properties of stable or unstable waves. The phase of the most unstable wave is only slightly reduced in the three bottom layers (2.6% in the bottom layer). As in Case 2, two-layer models are much more sensitive (Walls 1989, personal communication). The fact that the complex amplitude depends only on the vertical coordinate; this also contributes to decrease the effect of bottom friction (A91). Numerical experiments with and without bottom friction but without lateral friction gave similar results.

In comparison with area I (Case 1), the areas II and III have weaker mean flows which imply less available potential energy. Thus fewer and less unstable waves are generated. As in Case 1, the most unstable wave also propagates southward, but with larger spatial and temporal scales and with a slightly slower phase speed (see Table 3).

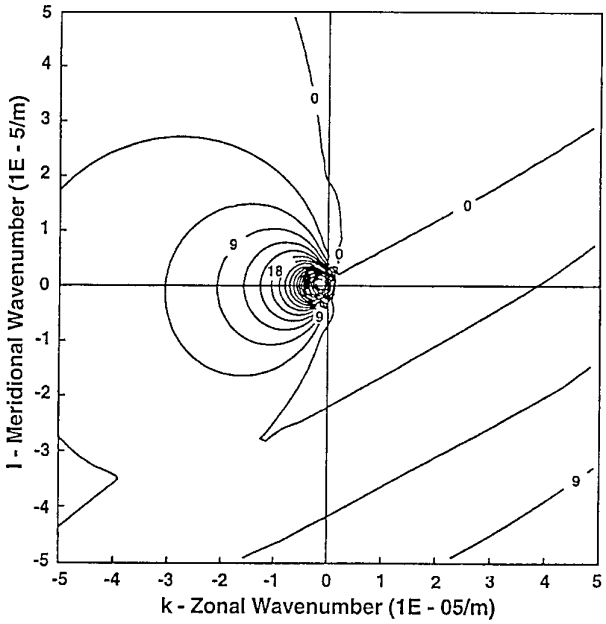

Fig. 7a. Dispersion relation for barotropic mode of stable waves for Case 2 (flat bottom). Contour interval = 3 x 10^{-7} s^{-1}.

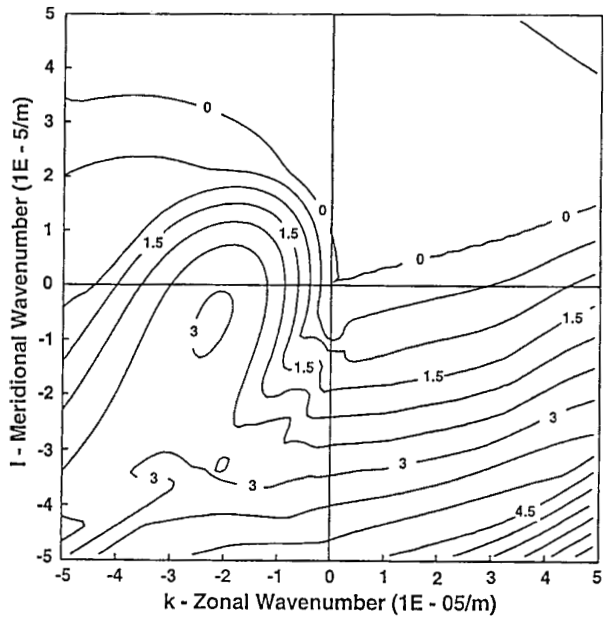

Fig. 7b. Dispersion relation for first baroclinic mode of stable waves for Case 2 (flat bottom). Contour interval = 5 x 10^{-8} s^{-1}.

The first baroclinic stable modes for areas II and III also present few changes with respect to area I, mainly at scales greater than the deformation radius. Group velocities and phase speeds are slower in area I than in areas II and III by about 25%. For first baroclinic waves of annual periods and stratification typical of the CC a critical latitude exists around

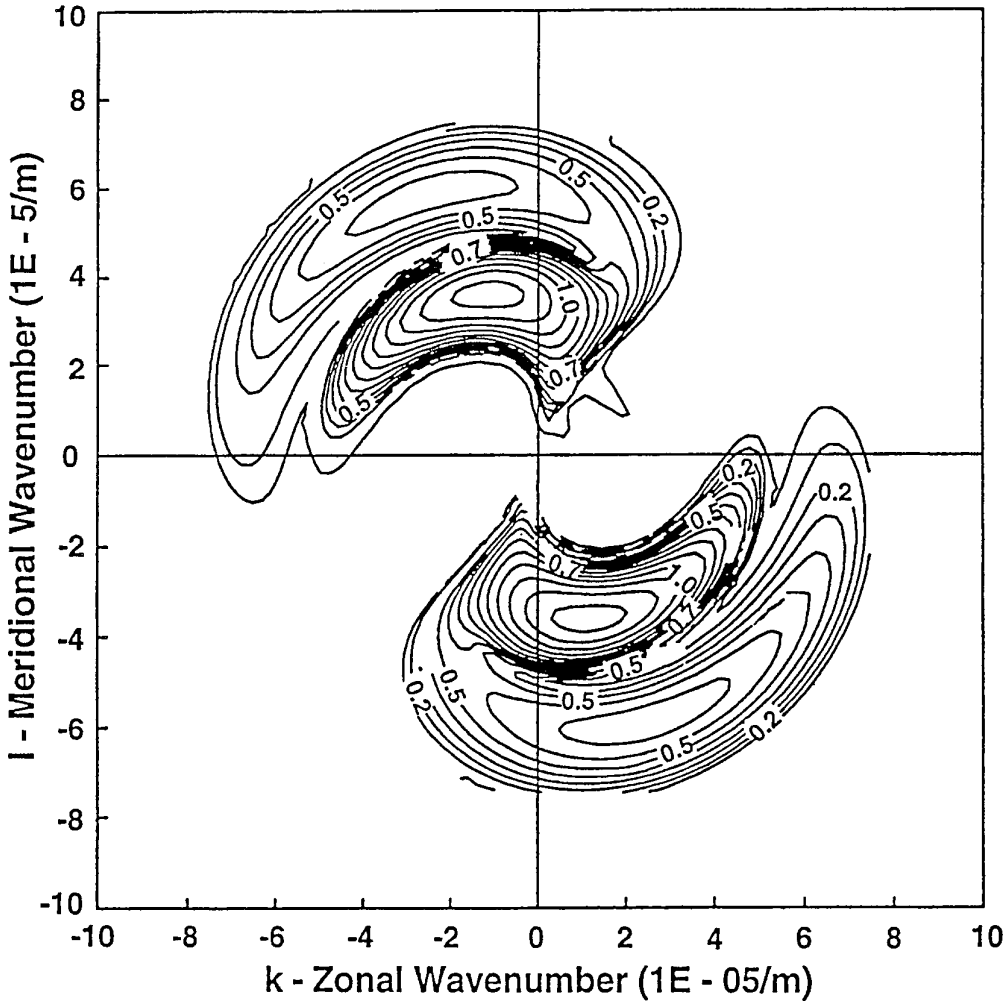

Fig. 8. Growth rates of unstable waves for Case 6 (area IV). Contour interval = 5 x 10^{-9} s^{-1}.

38° N (McCreary *et al*. 1987). Poleward of this critical latitude, the waves have an exponential decay that limits offshore propagation. This can be seen by solving for *k*, the zonal wavenumber, from the Rossby wave dispersion relation. Area I is very close to this critical latitude which might explain the very slow propagation speed observed in this area, as compared to areas II and III. A critical latitude in a reduced gravity formulation was detected by Parés-Sierra (1991) from the propagation patterns of model waves. For a reduced-gravity model forced by observed winds (COADS, dominated by the annual period variability) a very clear dichotomy exists in the propagation of the waves. Perturbations propagate equatorward of about 35° N and decay poleward (Parés-Sierra, 1991). A much slower phase propagation at 38° N than at either 25° N, 28° N or 33° N was also found in A89.

The long Rossby waves found by A89 between the latitudes of 28° N and 33° N approximately match the dispersion relations shown here. The bidimensional spectra in A91 show waves with a period of 376 days and zonal wavelengths of 1960 km and 1550 km at 28° N and 33° N respectively. Between these two latitudes (our Area III), and for these two wavelengths, we obtain wave solutions with periods of 450 days and 403 days respectively.

d. Case 7

In this case we study an area with a very different mean flow structure to the control calculation (Case 1). The main difference is that Area IV has an almost westward mean flow. This will dramatically change, with respect to Area I, the characteristics and dispersion properties of the waves.

Area IV has the most unstable waves of all cases. This agrees with results presented by A89, who found the greatest production of eddy kinetic energy by baroclinic instabil-

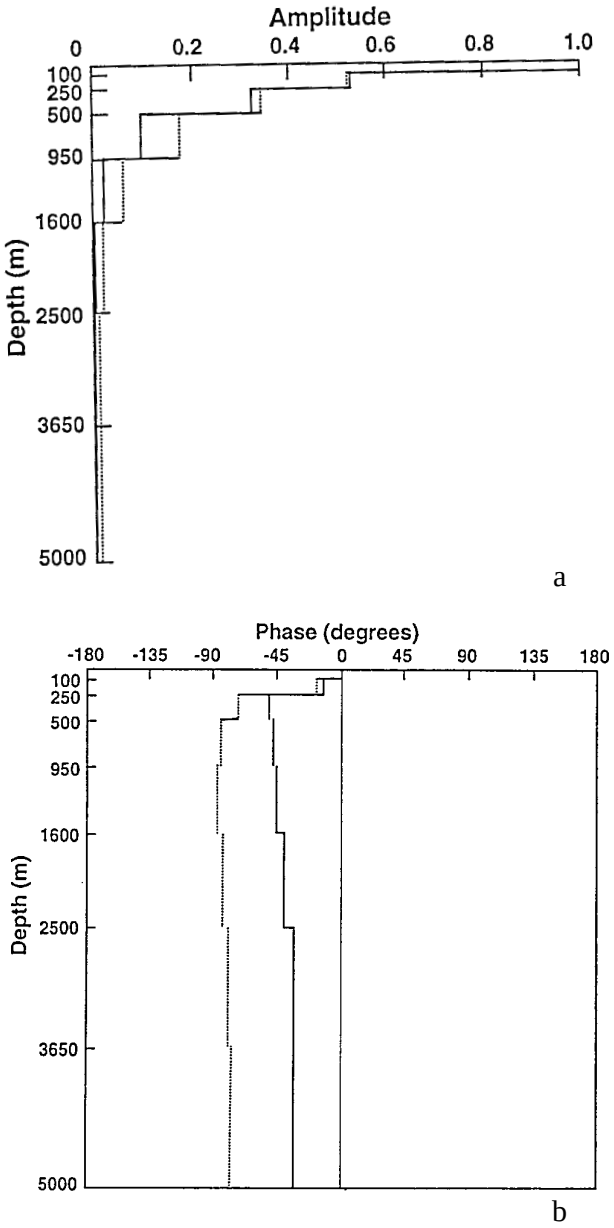

Fig. 9. a) Amplitude vs. depth of the MUW of Case 6 (area IV, solid line) vs. the MUW of Case 1 (area I, dotted line.), b) As in a) but for phase vs depth.

ity. The higher production of eddy kinetic energy is due to the direction of the surface mean flow in the top three layers. As noted by several authors, westward mean flows are unstable due to the fact that they easily satisfy the necessary conditions for the occurrence of baroclinic instability (see for example Kang *et al.*, 1982; Gill 1982). Our growth-rate field (Figure 8) shows good qualitative and quantitative agreement with Lee (1988) for a three-layer ocean.

The most unstable wave barely feels the topographic effect in comparison to areas I, II and III. This is because the wavenumber and topography gradient vectors form a smaller angle (see Figure 11). The amplitude and phase of the most unstable wave for area IV and area I are presented in Figure 9. It is seen that the most unstable wave of area IV is more baroclinic and has a larger vertical scale of decay for eddy kinetic energy than in Case 1. Despite the larger deformation radius of area IV, its most unstable wave has a horizontal scale smaller than area I (Case 1). This can be attributed to the different vertical structure of the mean flow rather than to the different latitudes as we should expect shorter waves in higher latitudes. The amplitude of the most unstable wave has a secondary maximum in the third layer (250 m-500 m) which could possibly be related to the absolute subsurface maxima observed in the southern part of the subtropical gyre (Lee and Niiler 1987).

The barotropic mode of this experiment does not differ markedly from the corresponding modes of Areas I, II and III. The mean flow velocity is very small in comparison with the phase speed of this mode. The dispersion relation for the first baroclinic mode (Figure 10) differs significantly from that in the other areas, where the surface mean flow is in the southeastward direction. In Area 7, the dominant mean flow is almost westward; it adds to the west-ward phase speed of the stable Rossby waves. The cut-off period is 180 days and is located at $K=(-2.3,0.6)\text{x}10^{-5}$ m^{-1}.

e. Linear vs. non-linear model

In this section we compare some results from the non-linear solution by A91 with their linear approximation. Linear baroclinic instability is caused by downgradient eddy fluxes of temperature, i.e. by mean flow instabilities, while non-linear baroclinic instability is due to convergences of the eddy flux of potential energy. Following A91, where the energy equation is studied in detail, these two contributions add up to a total vertical flux of temperature

$$\overline{W'T'^2} = -\frac{1}{2}\nabla\cdot\overline{VT'^2} - \overline{V'T'}\cdot\nabla\overline{T} \qquad (9)$$

where w, V and T are the vertical velocity, the velocity vector and the temperature. Primes denote anomalies with respect to the mean, and bars denote mean values. In the second term V is the total vector flow, i.e. the mean plus the perturbation. Thus, a vertical heat flux $w'T' > 0$ leads to baroclinic instability, i.e. a conversion of potential energy into eddy kinetic energy. Either the eddy flow is extracting potential energy from the mean flow (last term), and/or there is a sink of eddy potential energy due to the total flow (second term). The reader is referred to Pedlosky (1979) for a detailed treatment of both types of instabilities and their joint effect (hybrid instability). A91 finds a dominance of linear "local"

baroclinic instability over non-linear baroclinic instability. This dominance is summarized in Table 4 (from A91), for the three upper layers. The only area where non-linear instabilities are important is area I. The remaining layers, for all four areas where, show an overwhelming dominance of linear instabilities. This dominance is to be expected given the small Rossby number.

A91 shows that there is an almost linear relationship between vertically integrated eddy kinetic energy and vertically integrated energy flux due to boundary fluxes plus baroclinic instability (linear plus non-linear). If we substract energy fluxes originated by non-linear baroclinic instability from the variable defined in the horizontal axis (Figure 11), it turns out that the effect on Figure 12 from A91 is minimal. Thus, in almost all areas of the CCs the production of eddy kinetic energy is mainly originated in linear baroclinic instability processes and only secondarily by boundary fluxes.

Table 4

Ratios of eddy kinetic energy production due to advection of available potential energy over eddy kinetic energy production due to downgradient fluxes, for the four selected regions and for the top three layers

	Area			
Layer	I	II	III	IV
1	6.00	0.60	0.12	0.21
2	1.25	0.30	0.09	0.12
3	0.60	0.13	0.62	0.07

Figure 12 shows the 2-D spectra of the eddy streamfunction of the upper layer (from A91). It overlaps the long stable wave approximation of the dispersion relations corresponding to the first two baroclinic modes. A spectral peak with a period of 376 days is very close, in all cases, to the first mode of the idealized waves. These waves are likely generated by the annual fluctuations of Ekman pumping, through the wind stress curl, along the eastern boundary of the North Pacific Ocean (White and Saur, 1981). The black dot on the left of Figure 12(a) corresponds to the location of the most unstable wave of area IV from the linearized model. Its location ω-*k* space is very close to the eddy energy secondary maxima from the 2-D non-linear model.

The upper 100m of the main part of the California Current (Area I) are the only ones dominated by non-linear baroclinic instability. This may be due to the strong eddy activity as shown by Lynn and Simpson (1988) and by A91. These eddies interact with each other. In the remaining areas and depth, shown in Table 4, the production of eddy variability is almost enterily due to the mean flow instability through a release of mean potential energy into eddy kinetic energy.

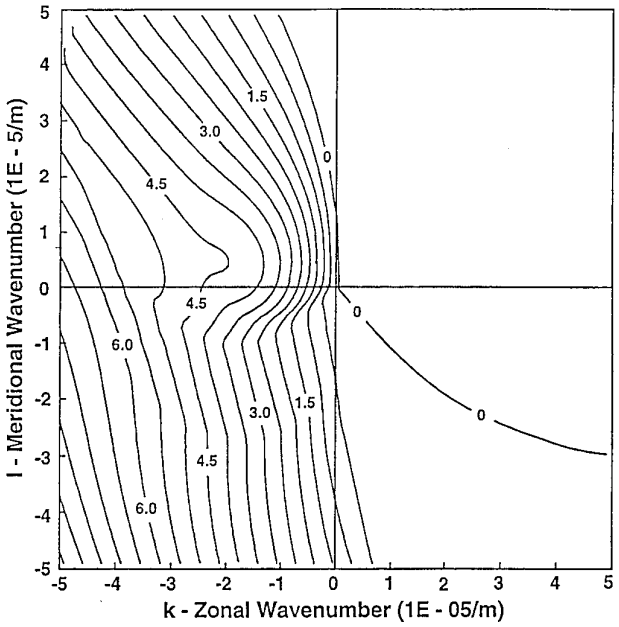

Fig. 10. First baroclinic mode of stable waves for experiment 7 (area IV). Contour interval = 5 x 10^{-8} s^{-1}.

In conclusion, Table 4 and Figures 11 and 12 suggest that the CCS may be represented by a linearized quasi-geostrophic model. The amount of eddy kinetic energy produces by barotropic instability processes is at least an order of magnitude smaller than the amount generated by baroclinic instabilities (A91).

IV. CONCLUSIONS

The complex eigenproblem of an 8-layer quasi-geostrophic model was solved numerically to study the properties of Rossby waves generated by baroclinic instability in the CCS. A realistic effect of topography and bottom friction requires a high vertical resolution. When the vertical resolution is low the effect of topography and bottom friction may affect the main thermocline directly in its stability properties, and the effects are imposed over a large section of the water column. Topography and bottom friction play a greater role in a two-layer model (e.g. Robinson and McWilliams, 1974) than in the present 8-layer one. Thus bottom friction

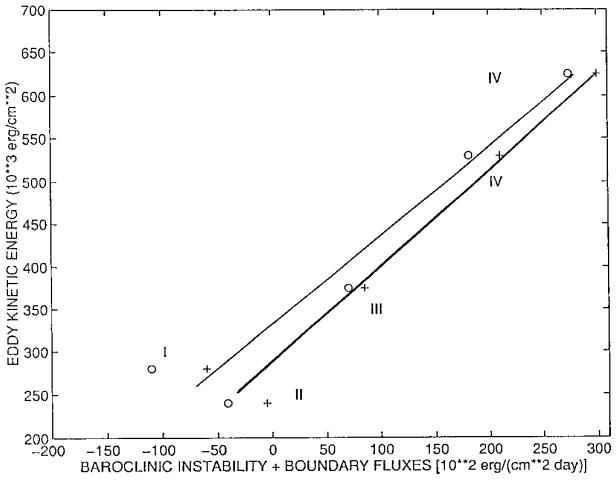

Fig. 11. Vertically integrated eddy kinetic energy vs. vertically integrated production of eddy kinetic energy by baroclinic instability plus boundary fluxes. The roman numbers indicate the selected area, the +'s refer to the case when the baroclinic instability contribution to the x axis takes into account both linear plus non-linear processes and the o's refer to the case when only linear baroclinic instabilities are added to the boundary fluxes. The heavy straight line is the best fit to the +'s and the light line is the best fit to the o'.

and bottom slope effects are artificially enhanced by poor vertical resolution. On the other hand, these effects will have a more important role in determining the wave properties in weakly stratified areas such as the Antartic Circumpolar Current.

The dispersion relations for the sloping bottom case suggest that stable Rossby waves had group velocities up to 60% faster than in the flat bottom case. The inclusion of a gently sloping bottom, typical of the northeastern Pacific ocean, enhances the beta effect and leads to shorter and thus more barotropic waves. It also increases the kinetic energy of the upper layers, relative to the deeper ones, due to the relative increase of the bottom slope effect over the β effect. This relationship between wave parameters leads to an increased dominance of the surface intensified Rossby waves over other types of Rossby waves, including bottom-trapped and shear-free waves, (see Rhines 1977, pp. 214). The surface-intensified mean flow also leads to surface intensified unstable waves since the release of available potential energy will be larger where the mean flow is faster and more sheared, i.e. above the thermocline which in this model is at 500 m. The growth rates were very similar in both cases.

A biharmonic frictional mechanism leads to more barotropic and smaller e-folding vertical scales for the kinetic energy of the most unstable wave. This is probably due to the different scales of the most unstable waves (166 km for the biharmonic frictional case and 296 km for the Laplacian case), rather than to higher-order frictional physics. Therefore, numerical models using a biharmonic frictional term, with values for the coefficients of lateral friction close to the ones in this article (Table 2), should provide shorter, more energetic and more barotropic variability than when using a Laplacian term.

The dispersion relation of the first baroclinic stable Rossby mode for area I (33° - 38° N) showed very good agreement with Kang *et al*. (1982) for the California Current. The growth rates are in good agreement with those of Lee (1988) and Lee and Niiler (1987). The quasi-linear first baroclinic-mode annual Rossby waves found in A91 (non-linear numerical model) have frequencies and wavenumbers that closely match the dispersion relations obtained with our linear model. Both indicate that Area IV is the most energetic of all four areas. This agreement is partly due to the fact that linear baroclinic instability dominates over non-linear baroclinic instability at most locations analyzed in A91.

The method used in this paper is strictly valid in the first stages of unstable Rossby waves. Yet some of these waves, especially those with long horizontal scales ($Ro << 1$) and large growth rates, may become dominant in the long run for a realistic non-linear ocean. The waves described in the seven cases are to be considered a first step in the study of temporal evolution of mesoscale variability for the CCS area.

ACKNOWLEDGEMENTS

This article benefited from the comments and suggestions of two anonymous reviewers. This work was supported by Mexico's Secretaría de Educación Pública, by CICESE, and by the Consejo Nacional de Ciencia y Tecnología under grant 0794-T9110. GA was supported by NOAA under the Scripps Experimental Climate Prediction Center a (NA67GPO450), the Lamont/Scripps Consortium for Climate Research (NA47GPO188), and the Paleoclimate Program (NA66GP0274). GA was also supported by the National Space Development Agency of Japan (NASDA), under a joint program entitled "Pacific Ocean Variations".

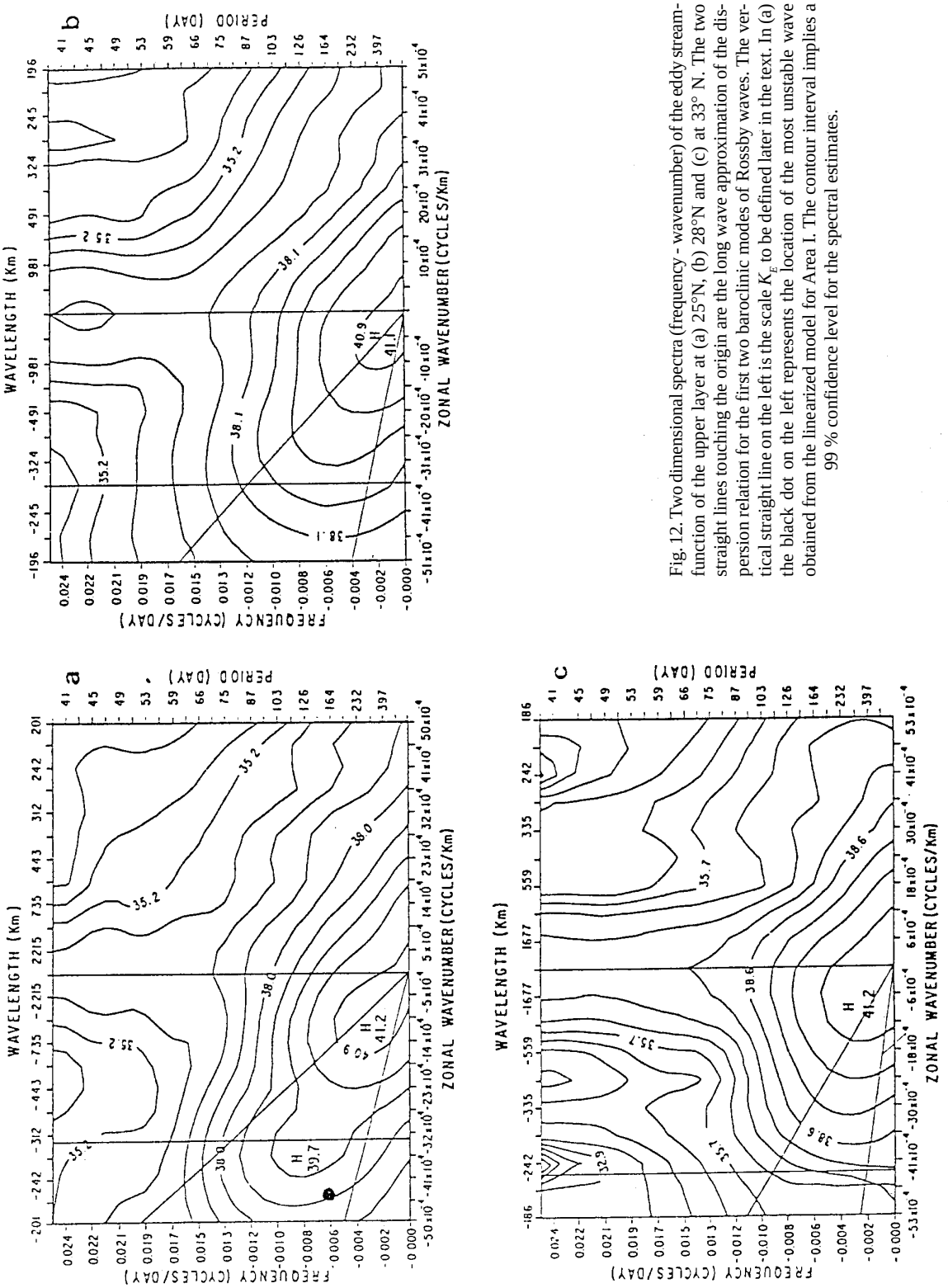

Fig. 12. Two dimensional spectra (frequency - wavenumber) of the eddy stream-function of the upper layer at (a) 25°N, (b) 28°N and (c) at 33° N. The two straight lines touching the origin are the long wave approximation of the dispersion relation for the first two baroclinic modes of Rossby waves. The vertical straight line on the left is the scale K_E to be defined later in the text. In (a) the black dot on the left represents the location of the most unstable wave obtained from the linearized model for Area I. The contour interval implies a 99 % confidence level for the spectral estimates.

BIBLIOGRAPHY

AUAD, G., A. PARES-SIERRA and G. VALLIS, 1991. Circulation and energetics of a model of the California Current System. *J. Phys. Oceanogr., 21,* 1534-1552.

AUAD, G., 1989. Estudio cuasi-geostrófico de la circulación inducida por el viento en el sistema de la Corriente de California. Ms. thesis. Centro de Investigación Científica y de Educación Superior de Ensenada, 125 pp.

CUSHMAN-ROISIN, B. and B. TANG, 1990. Geostrophic turbulence and emergence of eddies beyond the radius of deformation. *J. Phys. Oceanogr., 20,* 97-113.

GILL, A. E., 1982. Atmosphere-Ocean Dynamics. Academic Press, 662pp.

HARRISON, D. E., 1980. Dissipation mechanism and the importance of eddies in mid-ocean energy budgets. *J. Phys. Oceanogr., 10,* 900-905.

HOLLAND, W. R., 1978. The role of mesoscales eddies in the general circulation of the ocean-numerical experiments using a wind-driven quasi-geostrophic model. *J. Phys. Oceanogr., 8,* 363-392.

HOLLAND, W. R. and G. K. Vallis, 1995. An eddy resolving model of the California Current nested in a model of the North Pacific. Unpublished manuscript.

KANG, Y., J. PRICE and L. MAGAARD, 1982. On stable and unstable Rossby waves in non-zonal oceanic shear flow. *J. Phys. Oceanogr., 12,* 528-537.

LEE, D. K., 1988. A numerical study of the non-linear stability of the eastern ocean circulation. *J. Geophys. Res., 93,* 10630-10644.

LEE, D. K. and P. P. NIILER, 1987. The local baroclinic instability of geostrophic spirals in the Eastern North Pacific. *J. Phys. Oceanogr., 17,* 1366-1377.

LYNN, R. and J. J. SIMPSON, 1988. The California Current System: the seasonal variability of its physical characteristics. *J. Geophys. Res., 92,* 12, 947-12, 966.

McCREARY, J. P., P. K. KUNDU and S. CHAO, 1987. On the dynamics of the California Current System. *J. Mar. Res., 45,* 1-32.

PARES-SIERRA, A. 1991. Remote and local forcing of Rossby wave variability in the midlatitude Pacific Ocean. *Geofís. Int. 30, 3,* 121-134.

PEDLOSKY, J. 1979. Geophysical Fluid Dynamics. Springer-Verlag, 624 pp.

RHINES, P.B., 1977. The dynamics of Unsteady Currents. The Sea, Vol 6, Wiley Interscience, 189-318.

ROBINSON, A. R. and J. McWILLIAMS, 1974. The baroclinic instability of the open ocean. *J. Phys. Oceanogr., 4,* 281-294.

WHITE, W. B. and J. F. SAUR, 1981. A source of annual baroclinic waves in the eastern subtropical North Pacific. *J. Phys. Oceanogr., 11,* 1452-1462.

Guillermo Auad[1] and Alejandro Parés-Sierra[2]

[1] Climate Research Division, Scripps Institution of Oceanography, La Jolla, CA 92093-0224, USA.

[2] Centro de Investigación Científica y Educación Superior de Ensenada, Km. 107, Carretera Tijuana-Ensenada, 22860 Ensenada, B. C., México.